Anti-corrosion and wear performance of Al-Si coating deposited by wire arc spray for marine applications

Minhye Kang[1] · Hansol Kwon[2] · Eungsun Byon[3] · Eunkyung Lee[†]

Abstract: Pure Al, Al-6Si, and Al-12Si coatings were deposited on HSLA-100 low-carbon steel substrates using wire arc spraying. The corrosion and wear behaviors of the Al and Al-Si coatings were investigated. It was observed that corrosion occurred preferentially in the aluminum matrix, and Si remained. The pit nucleation resistance decreased as the Si content increased. An immersion test revealed that the Al-12Si coating exhibited the lowest average weight loss. Wear tests were conducted on the uncorroded and corroded surfaces of the coatings to investigate the wear performance with complex corrosion characteristics. The Al-12Si coatings exhibited the highest wear resistance under both uncorroded and corroded conditions. The wear mode of the Al-Si coatings transitioned to fatigue wear caused by significantly high local shear stress applied to the edges of the pits.

Keywords: Al-Si coatings, Sliding wear, Thermal spray, Corrosion behavior, Marine environment

1. Introduction

Low-carbon steel is widely used in vehicle parts, building materials, and subsea construction owing to its good mechanical properties and low price compared with high-alloyed steel. However, in marine environments, contact with seawater significantly increases the risk of corrosion by Cl ions and dissolved oxygen. This causes early destruction. Most materials used in marine environments undergo wear owing to the waves and sand, which results in mechanical and chemical interactions. This interaction causes steel to corrode more rapidly than in static environments. To prevent surface damage, the addition of alloy elements or surface processing is required for low-carbon steels to ensure corrosion and wear resistance.

Thermal spraying is a process in which a powder or wire-type material is melted using a heat source and then, sprayed onto the surface of a substrate material at a high speed to form a coating layer [1]-[2]. It is one of the most widely used coating processes because it is environmentally friendly and simple, and improves the corrosion and wear resistance of the material [3]-[5]. Thermal sprayed aluminum is a durable coating material used in arc wire spray, high-velocity oxygen fuel (HVOF), and flame spray.

Aluminum is primarily used as a spray coating material to prevent corrosion. It is lightweight and has a low melting point, which is suitable for use as a spray material [6]. In particular, when aluminum is exposed to low-carbon steel, it generally has a lower corrosion potential than steel and functions as a sacrificial cathode to protect the steel [7]-[8].

An oxide film naturally forms on an aluminum surface and protects the aluminum from corrosion damage [9]-[10]. However, pitting corrosion is a major issue in the use of aluminum under subsea conditions where Cl ions exist. Chloride ions can destroy the oxide film on the aluminum surface and thereby, cause pitting corrosion [11]. However, the use of pure Al as a coating material is limited because of its low mechanical strength [12]. Alloying elements are required to overcome this problem. Al-Si alloys are the most commonly used commercial aluminum alloys. Si has the advantage of improving the castability and bonding properties by improving the flow of molten metal [13]-[14]. It has a

† Corresponding Author (ORCID: http://orcid.org/0000-0003-0723-8524): Associate Professor, Interdisciplinary Major of Maritime AI Convergence, Department of Ocean Advanced Materials Convergence Engineering, 727, Taejong-ro, Yeongdo-gu, Busan 49112, Korea, E-mail: elee@kmou.ac.kr, Tel: 051-410-4353

1 M. S., Interdisciplinary Major of Maritime AI Convergence, Department of Ocean Advanced Materials Convergence Engineering, Korea Maritime & Ocean University, E-mail: minhye1228@naver.com, Tel: 051-410-4955

2 Ph. D., Surface Materials Division, Department of Extreme Environmental Coatings, Korea Institute of Materials Science, E-mail: hskwon@kims.re.kr, Tel: 055-280-3645

3 Ph. D., Surface Materials Division, Department of Extreme Environmental Coatings, Korea Institute of Materials Science, E-mail: esbyon@kims.re.kr, Tel: 055-280-3555

Minhye Kang ・ Hansol Kwon ・ Eungsun Byon ・ Eunkyung Lee

significantly low solubility of 0.1 at. % at 150 °C to form a eutectic system. Moreover, the shape and distribution of eutectic Si vary depending on the Si content. The content, size, shape, distribution, and the like of Si in the Al alloy are a few main factors that affect the mechanical characteristics. In particular, when Si is spherical, it has an anisotropic microstructure. This increases the wear resistance [15]-[16].

Several studies have been conducted on the effects of adding Si to Al alloys, on corrosion and wear. It is established that an Al-Si coating forms dense corrosion products from Al and Si. Thus, it exhibits corrosion resistance through a barrier effect. According to Reynier I. Revilla, when Al-Si alloys with different Si contents are deposited, the Si eutectic network can protect the Al matrix from corrosion and increase the corrosion resistance [17]-[18]. In addition, Si prevents the generation of FeAl intermetallic compounds in the intermetallic layer of the coating and reduces the layer thickness by delaying the diffusion rate of Al into the steel in the solid phase [19]. However, according to K.M. Fleming, Si can exist as an anode in the Al matrix. This results in galvanic or local corrosion [20]. The main causes of wear in Al-Si alloys are the size of the dendrites, aspect ratio, and distribution of the Si phases [21]. A study investigating the variation in the wear characteristics of Al alloys according to the Si content, distribution, and shape revealed that the size and distribution of Si significantly affected the wear mechanism [22]. Mahato and Warmuzek noted that the addition of Si particles improved the wear characteristics of hypereutectic Al-Si alloys [23]-[24].

The dependence of the electrochemical properties on the Si content of the Al coating prepared using WAS has not been identified clearly. In addition, although corrosion is accompanied by wear in marine environments, most studies on the corrosion and wear resistance of Al-based coatings have been conducted independently. Therefore, this study investigated the wear and corrosion characteristics of wire arc-sprayed Al-Si coatings. Electrochemical experiments were conducted on pure Al, Al-6Si, and Al-12Si coatings to evaluate the corrosion resistance of the coating materials. Wear tests were conducted on the uncorroded and corroded surfaces of the coatings to compare and analyze the effect of the corrosion reaction on the wear phenomenon.

2. Experimental Procedure

2.1 Material

HSLA-100 steel was used as the substrate material. Its chemical composition is listed in **Table 1**. Prior to coating, the substrate

alloys were grit-blasted using white alumina powder with a grit size of 20 mesh. Pure Al, Al-6Si, and Al-12Si wires were used as feedstock materials. Al and Al-6Si were coated using the ARCJET 99/600 PL SPRAY SYSTEM. Meanwhile, Al-12Si was coated using the Metco SMART ARC SYSTEM. **Table 2** lists the parameters of the coating process for each specimen. The average surface roughness was calculated by measuring the surface roughness three times in the same area using a high-resolution optical 3D surface analyzer (VHX-7000, KEYENCE). The surface roughness Ra of the Al, Al-6Si, Al-12Si coatings was 14.00 μm, 19.93 μm, and 14.37 μm, respectively.

Table 1: Chemical composition of HSLA-100 (wt. %)

Elements	Fe	Ni	Cu	Cr	Mo	Mn	Si	C
HSLA-100 (substrate)	Bal.	3.5	1.3	0.6	0.5	0.5	0.2	0.05

Table 2: Parameters for wire arc spraying of metallic coatings

	Al	Al-6Si	Al-12Si
Voltage (V)	32	32	38
Arc current (A)	150	150	280
Air pressure (psi)	72.5	72.5	80
Spray distance (mm)	130	130	150

2.2 Electrochemical measurements

The corrosion resistance of the coatings was determined via electrochemical testing. Electrochemical cyclic potentiodynamic polarization measurements and galvanic corrosion tests were conducted in a 3.5% NaCl solution using a potentiostat (Interface 1010E Potentiostat, Gamry Instruments, USA). Cyclic potentiodynamic polarization was performed using a three-electrode cell with a saturated calomel electrode (SCE) as the reference electrode, platinum counter electrode, and coating working electrode. The area of the working electrode exposed to the solution was 1 cm². Cyclic potentiodynamic polarization was conducted from -500 mV to 1100 mV at a scan rate of 0.1 mV/s after stabilization for 60 min.

2.3 Immersion tests

The Al-, Al-6Si-, and Al-12Si-coated specimens were immersed in a 3.5 wt. % NaCl solution for 14 days. The surface area exposed to the solution was 6.36 cm². It was polished to #2400 grit prior to the immersion. Three test specimens were prepared for each coating composition and immersed under identical conditions. After the immersion tests, the surfaces were rinsed with

distilled water and dried. The weight before and after immersion was measured using a digital balance.

2.4 Mechanical tests

A Vickers hardness test was performed on the surface of the coatings to analyze the hardness of the coating layer according to each composition. A micro-Vickers hardness tester (HM-122, Akashi, Japan) was used for the hardness tests. Before the test, the surfaces of all the coatings were polished to #2400 grit using SiC sandpaper. The specimens were pressed for 10 s with a load of 0.1 kgf, and the hardness was calculated by measuring the indentation area. To evaluate the wear resistance of the coating depending on whether it was corroded, wear tests were conducted on the uncorroded coating surface and the coating surface after 14 days of immersion experiments. The experiment was conducted using the ball-on-disc dry sliding method with a wear tester (102 PD; R&B, Korea). The wear tests were conducted three times for each condition. The experimental conditions are listed in **Table 3**. A stainless steel 304 ball with a diameter of 6 mm was used as the counter material. The uncorroded coating surfaces were polished to #2400 grit using SiC sandpaper, and a wear test was performed.

Table 3: Wear test experimental condition

Parameter	Condition
Temperature (°C)	25 (Room temperature)
Load (N)	30
Sliding speed (rpm)	100
Time (min)	30
Rotation diameter (mm)	11.5

Archard's equation was used to measure the specific wear rate, $k = V / (F \cdot L)$. V is the volume of the worn material, F is the normal load, and L is the sliding distance. The wear tests were conducted under identical conditions on three test specimens for each composition and corrosion occurrence. The weights before and after wear were measured and divided by the density according to the composition to obtain the worn volume. Then, the wear rate was calculated.

2.5 Microstructure analysis

The microstructure of the coatings was observed on the cross-section using field-emission scanning electron microscopy (FE-SEM, CLARA) with energy-dispersive X-ray spectroscopy (EDS, EDAX). At least ten fields were averaged to measure the porosity area fraction using an image analyzer. To measure the wear depth, 3D profiling was performed in the depth direction from the worn surface using a high-resolution optical 3D surface analyzer (VHX-7000, KEYENCE).

3. Results and discussion

3.1 Characterization of the coatings

SEM micrographs of the cross-sections of the Al, Al-6Si, and Al-12Si coating layers are shown in **Figure 1**. The Al and Al-6Si coating layers had relatively uniform morphologies compared with the Al-12Si coating. As shown in **Figure 1 (c)**, the Al-12Si coating layer consisted of a large number of oxides, pores, and cracks.
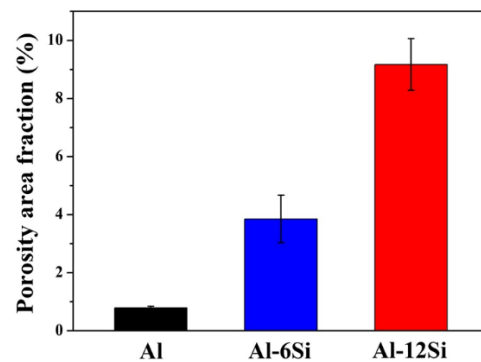

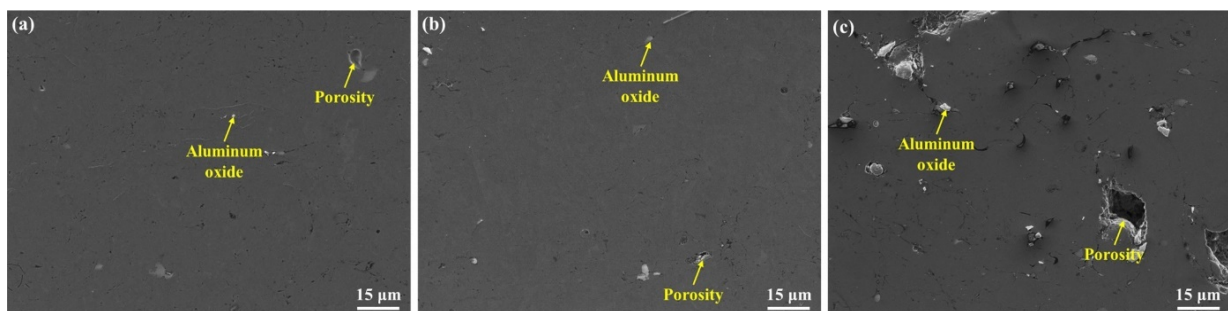**Figure 2:** Average porosity area fraction of Al, Al-6Si, and Al-12Si coatings

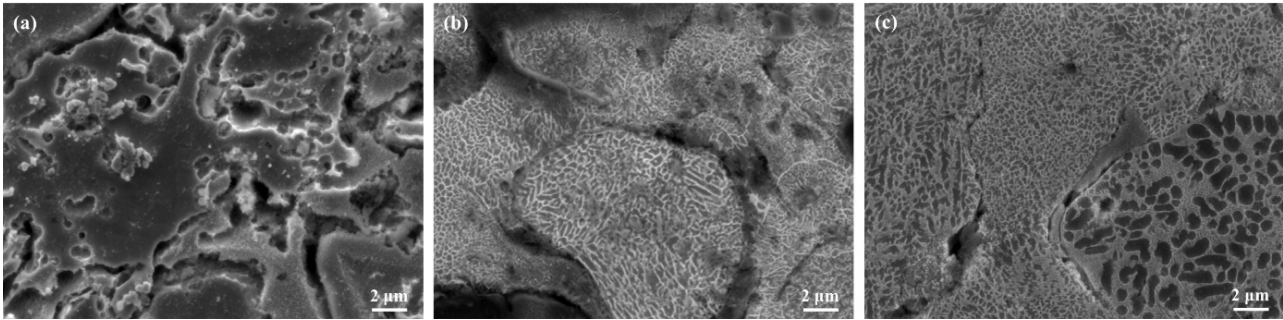**Figure 1:** Cross-sectional micrographs of (a) Al, (b) Al-6Si, and (c) Al-12Si coating

Minhye Kang · Hansol Kwon · Eungsun Byon · Eunkyung Lee

Figure 3: Surface microstructure of (a) Al, (b) Al-6Si, and (c) Al-12Si coatings

Figure 2 shows the average porosity area fraction in the cross-sections of the Al, Al-6Si, and Al-12Si coatings. The standard deviations are represented by error bars. The porosity increased significantly as the Si content increased. The average porosity area fractions of the Al, Al-6Si, and Al-12Si coatings were approximately 0.79%, 3.85%, and 9.17%, respectively. During the coating process, when the arc current is insufficient or the spray distance increases significantly, the temperature of the spray particles decreases to form a splat. This causes an insufficient plastic deformation. When the plastic deformation is insufficient, the interfacial bonding between the splats weakens. This results in porosity.

Figure 3 shows the SEM micrographs of the surface microstructure observed after etching the surfaces of the Al, Al-6Si, and Al-12Si coatings. After etching using the Keller solution, a distinction between the splats present on the coating surface was evident. The formation of eutectic Si was verified in the Al matrix. As shown in the micrographs of the Al-Si coating in **Figure 1 (b)** and **(c)**, eutectic Si with a relatively high brightness was finely distributed in a net-like form. In addition, the distribution differed depending on the Si content. Eutectic Si was more densely distributed on the Al-12Si coating surface than on the Al-6Si coating. Moreover, the distribution of Si differed between the splats constituting the coated layer. A few splats had a fairly dense net-like shape, whereas the others had a relatively larger net-like form of eutectic Si. The forms of Si distribution differed depending on the splat. The cooling rate of each splat was influenced by its thickness, the sprayed surface state, and the thermal characteristics of the material **[25]**. Moreover, the Si distributions of different forms were caused by the difference in cooling rate that occurs naturally during the coating process.

3.2 Corrosion performance
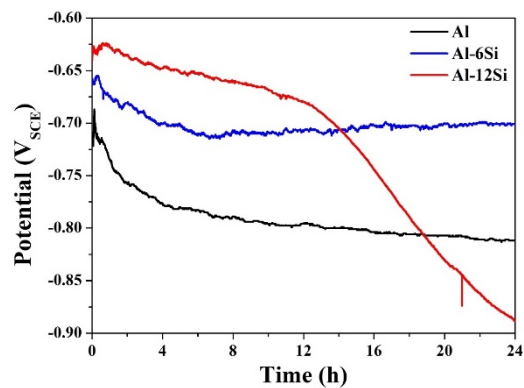
3.2.1 Open circuit potential

Figure 4: Open circuit potential of Al, Al-6Si, and Al-12Si coatings

Figure 4 shows the open-circuit potentials of the Al, Al-6Si, and Al-12Si coatings. The test was conducted for 24 h to observe the initial corrosion behavior. The Al coating exhibited the lowest initial corrosion potential of -0.719 V. Then, its potential increased dramatically. It again revealed a decreasing trend. This is attributed to the barrier effect of the initially generated oxide film **[30]**. The corrosion potential increased to -0.687 V, displayed a weak fluctuation until 34 min, and then decreased steadily. Al-6Si also exhibited a behavior in which the corrosion potential increased and then decreased marginally in the initial stage, and started to increase gradually after 8 h. In the case of the Al-12Si coating, the corrosion potential was highest in the early stage. However, it decreased gradually. Then, the corrosion potential began to decrease rapidly after 12 h. The Al-12Si coating had a relatively large number of pores in the coating layer. These were exposed as the corrosion progressed. When pores exist, the surface area becomes larger owing to the porosity, and the area that reacts with the electrolyte increases. Therefore, the corrosion potential is likely to decrease rapidly. Moreover, the pores can function as a passage through which the electrolyte may pass, and the electrolyte may contact the substrate material to form a galvanic cell.

3.2.2 Cyclic potentiodynamic polarization

Cyclic potentiodynamic polarization (CPDP) was conducted to investigate the pitting corrosion behavior of the coatings. **Figure 5** shows the CPDP curves of the Al, Al-6Si, and Al-12Si coatings. The corrosion potential shifted in the positive direction as the Si content increased. It is considered that Si has a relatively electronegative property with a noble corrosion potential, which affects the corrosion potential of the Al-Si coating layer. The Al and Al-Si coatings revealed that the repassivation potential was located in a negative direction compared with the corrosion potential. This implied that the three types of coatings were vulnerable to pitting corrosion owing to the unstable repassivation.
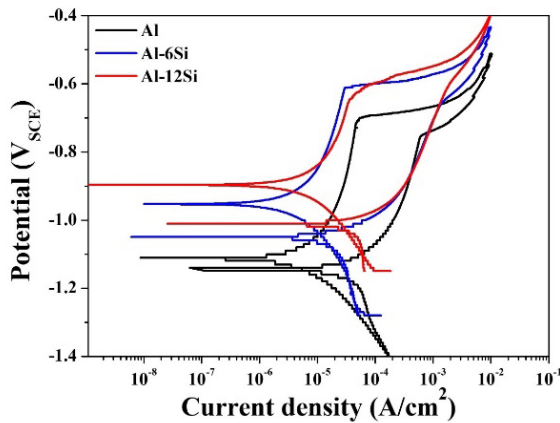

Figure 5: Cyclic potentiodynamic polarization curves of Al, Al-6Si, and Al-12Si coatings

Table 4: Cyclic polarization corrosion parameters

	E_{corr} (mV$_{SCE}$)	I_{corr}(μA/cm^2)	E_{pit}-E_{corr} (mV$_{SCE}$)
Al	-1110	13.3	398
Al-6Si	-953	15.8	341
Al-12Si	-897	22.1	247

Table 4 shows the corrosion parameters derived from the cyclic polarization curves. Based on the results presented in the table, the corrosion potential of each of Al, Al-6Si, and Al-12Si coatings was -1110 mVSCE, -953 mVSCE, and -897 mVSCE. The current density of the Al coating was the lowest (13.3 μA/cm^2), and those of the Al-6Si and Al-12Si coatings were 15.8 μA/cm^2 and 22.1 μA/cm^2, respectively. As the Si content increased, the current density increased. Corrosion is generally considered to occur gradually at low current densities. However, the corrosion rate determined from polarization with Tafel extrapolation is unreliable because of the anodic hydrogen

evolution [26][33]. Furthermore, in the case of the Al-Si coating with a higher porosity, the actual surface area in contact with the electrolyte increased. E_{pit} - E_{corr} in **Table 4** is the difference between the pitting potential and corrosion potential, which is an indicator of the pit nucleation resistance [30]. The pit nucleation resistance decreased as the Si content increased. This indicated that corrosion in the Al-12Si coating is highly likely to cause pitting corrosion. Similarly, the cyclic polarization curve of the Al-12Si coating in **Figure 5** shows that the pitting potential was not evident after the passive region.
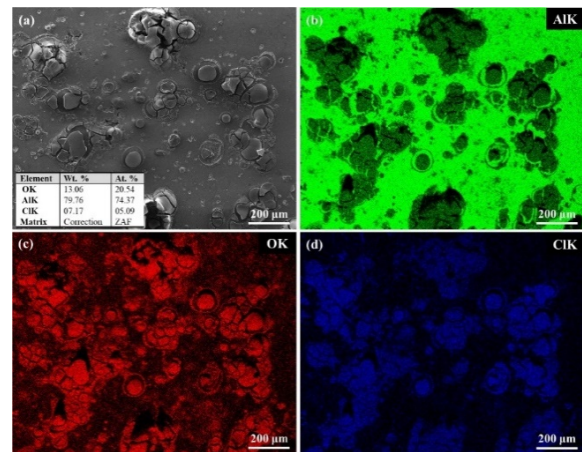

Figure 6: EDS mapping results of Al coating after cyclic polarization

The EDS mapping results for the Al, Al-6Si, and Al-12Si coatings after the CPDP test are presented in **Figures 6-8**, respectively. The round corrosion products on the Al coating surface agglomerated (**Figure 6**). These contained O and Cl, as detected by EDS mapping. The chloride constituent is considered to have been caused by the NaCl solution. The Al-6Si coating was characterized by a pitting attack, as shown in **Figure 7**. Al functioned as a preferential site susceptible to corrosion, whereas Si remained with O and Na. Similarly, the corroded Al-12Si coating morphology reveals preferentially corroded Al (**Figure 8**). It can also be observed that the Al-6Si coating experienced more severe corrosion than the Al-12Si coating with a deeper corroded morphology. The corrosion products of Al-Si alloys contained SiO$_2$. Furthermore, protective films with corrosion resistance obstruct the penetration of Cl- ions [31][32]. The distribution of eutectic Si affects the corrosion properties of Al alloys. Eutectic Si as a cathode results in the formation of a microgalvanic cell, which accelerates the corrosion of the Al matrix [34]. However, the dense network of eutectic Si prevents corrosion from spreading
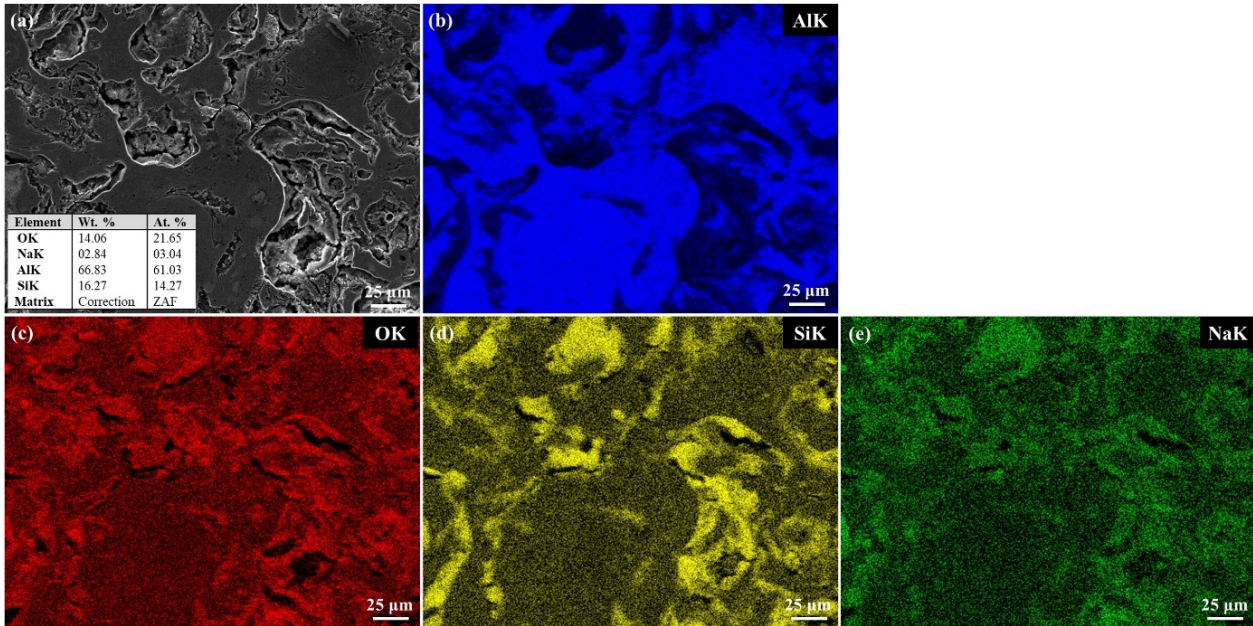
Minhye Kang · Hansol Kwon · Eungsun Byon · Eunkyung Lee

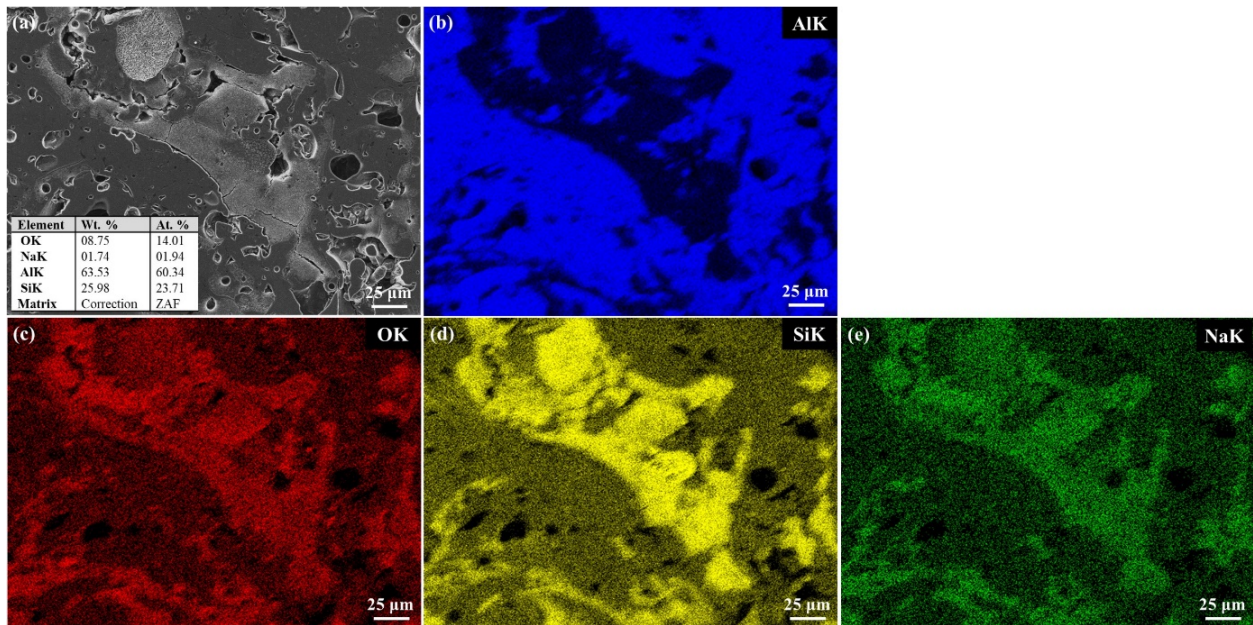**Figure 7:** EDS mapping results of Al-6Si coating after cyclic polarization

Figure 8: EDS mapping results of Al-12Si coating after cyclic polarization

Table 5: Weight loss of Al, Al-6Si and Al-12Si coatings

	Average weight loss (g)
Al	0.1767 ± 0.0206
Al-6Si	0.2667 ± 0.0544
Al-12Si	0.0300 ± 0.0082

into the matrix **[26]**. It was revealed that the finer Si structure in the Al-12Si coating resulted in a corrosion resistance better than that of the Al-6Si coating.

3.2.3 Immersion test

Table 5 shows the average weight loss values of the specimens immersed in a 3.5 wt. % NaCl solution for 14 days.

The standard deviations are indicated by the plus-minus symbol in **Table 5**. The average weight loss of the Al, Al-6Si, and Al-12Si coatings was 0.1767 g, 0.2667 g, and 0.0300 g, respectively. That is, the Al-12Si experienced the smallest weight loss. **Figure 9** demonstrates the microstructure of the Al, Al-6Si, and Al-12Si coatings after immersion in the 3.5 wt. % NaCl solution for 14 days. For the Al coating, most of the coating layer corroded away. Only a sponge-like structure remained (**Figure 9(a)**). The Al-O corrosion products were placed between the corroded structure. This was also observed in the Al-6Si coating (**Figure 9(b),(d)**).
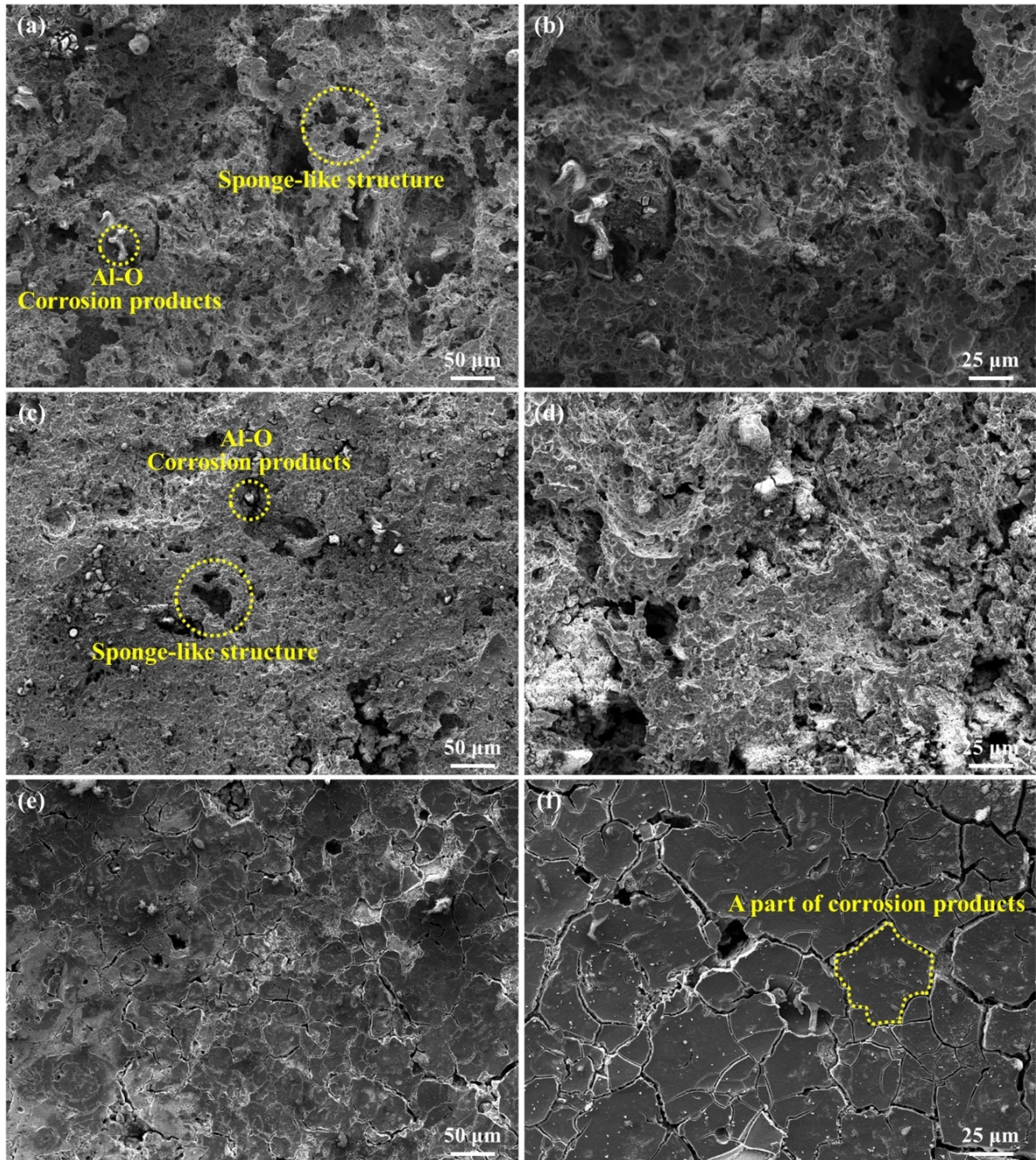
Figure 9: SEM Micrographs of coatings after immersion test for 14 days in 3.5 wt. % NaCl solution: (a), (b)Al; (c), (d) Al-6Si; and (e), (f)Al-12Si coatings

The corrosion products did not exist uniformly and stably in the form of small particles. Thus, the corrosion of the coating layer could not be prevented from proceeding. Similarly, in the Al-6Si coating, a sponge-like structure remained after the corrosion attack (**Figure 9(c)**). The immersed Al-12Si coating was observed to be covered with corrosion products (**Figure 9(e),(c)**). An EDS analysis was performed to clearly verify this in **Figure 10**. The corroded surfaces were composed of Al, Si, and O. It was

verified that the components of O were high at 49.07 at. %. Al, O, and Si were detected in the locations appearing as rigid corrosion products. It was observed that Si existed in the cracks between the corrosion products. This indicated that the α-Al matrix corroded rapidly.

3.3 Microhardness

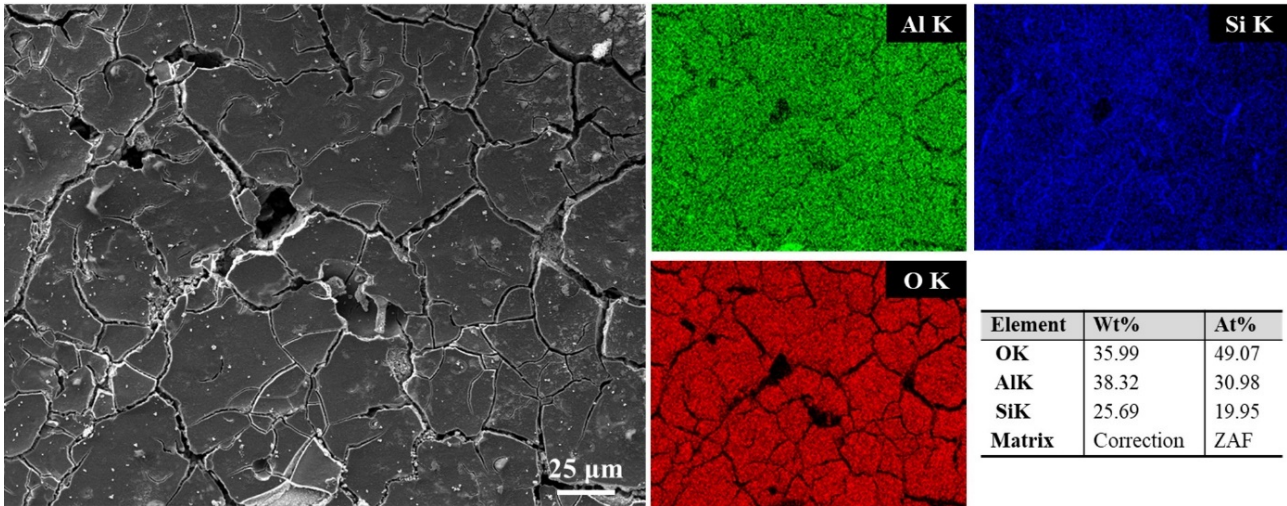The Vickers hardness test was conducted to investigate the

Minhye Kang ・ Hansol Kwon ・ Eungsun Byon ・ Eunkyung Lee

Figure 10: EDS results of immersed Al-12Si coating surface for 14 days in 3.5 wt. % NaCl solution

Element	Wt%	At%
O K	35.99	49.07
AlK	38.32	30.98
SiK	25.69	19.95
Matrix	Correction	ZAF

hardness properties of the Al and Al-Si coatings. **Table 6** shows the average hardness values and their standard deviations. The hardness increased with an increase in the Si content. The average hardness of the Al coating was the lowest (approximately 57.7 HV). As the Si content increased, Al-6Si and Al-12Si displayed hardness values of 121.9 HV and 179.0 HV, respectively. The hardness of the Al-12Si coating was approximately three times higher than that of the Al coatings.

Table 6: Vickers hardness value of Al, Al-6Si and Al-12Si coatings

	Average Vickers hardness (HV)
Al	57.77 ± 3.32
Al-6Si	121.85 ± 2.42
Al-12Si	178.96 ± 3.69

3.4 Wear performance

Figure 11 shows the average wear rates of the coatings under each condition. For the uncorroded Al, Al-6Si, and Al-12Si coatings, the wear rate decreased linearly as the Si content increased. The wear test was conducted after immersing the Al, Al-6Si, and

Al-12Si coatings in a 3.5 wt. % NaCl aqueous solution for 14 days. It was observed that as the Si content increased, the wear rate decreased. After 14 days of immersion, the wear rate increased in the Al, Al-6Si, and Al-12Si coatings. This tendency was most significant in the Al-6Si coatings. The wear rate of corroded Al-6Si coating increased by the most as compared to uncorroded coatings. This is considered to be mostly a result of the damage caused by corrosion. However, in the case of the Al coating, the difference in the wear rate depending on the corrosion

was relatively small. Additionally, the Al-12Si coating displayed a marginal difference in the wear rate after the immersion test.
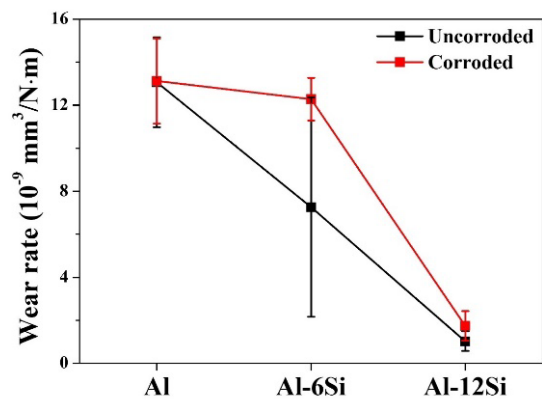

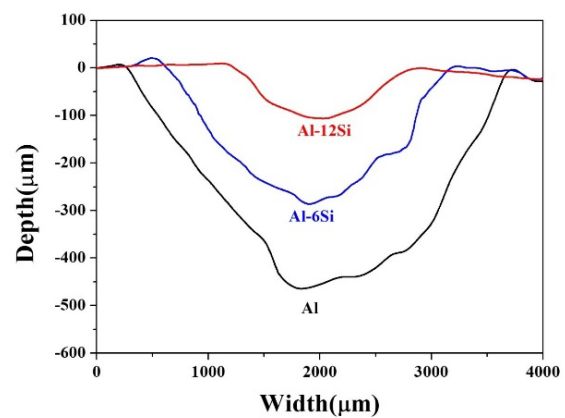**Figure 11:** Average wear rate of uncorroded and corroded coatings after immersion for 14 days

Figure 12: Depth profile of wear track of Al, Al-6Si and Al-12Si coatings
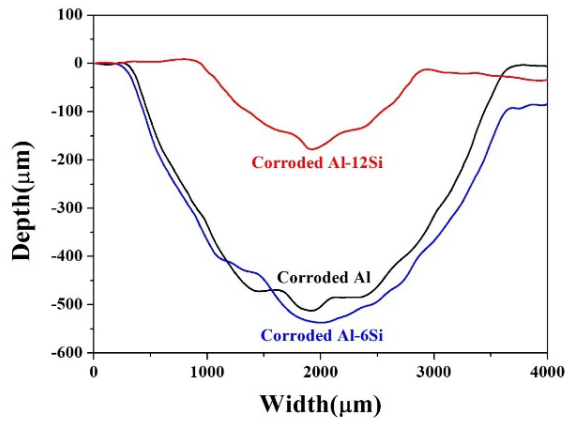
Figure 13: Depth profile of wear track of corroded Al, Al-6Si and Al-12Si coatings after immersion in 3.5 wt. % NaCl solution for 14 days

Wear depth profiling of the coatings was performed. **Figure 12** shows the profiling results for the uncorroded coatings. It was visually verified that the wear depth decreased as the Si content increased. This displays a tendency similar to that of the decrease in the amount of wear in the order Al, Al-6Si, and Al-12Si coatings. It can also be observed that the wear track width decreased with an increase in the Si content. **Figure 13** shows the results of wear depth profiling of the corroded coatings. The wear depth of the Al-12Si coating was the smallest. The wear depth increased in the order of Al and Al-6Si. For the corroded Al-6Si coating, the wear depth increased significantly. This coincides with the increased wear rate after corrosion.

To analyze the wear mechanism of the Al and Al-Si coatings, the coating surface was observed after the wear test using a scanning electron microscope. **Figure 14** shows a micrograph of the worn surfaces of the uncorroded and corroded coatings after the wear tests. Adhesive wear occurred on the worn surface of the non-corroded Al coating (**Figure 14(a)**). This was verified by the adhesive traces identified in the surface micrographs. The Al coating had the lowest hardness value (57.7 HV). Moreover, the coating layer appeared to have fallen off rapidly owing to the wear phenomenon on the surface with the counter material at a load of 30 N. Meanwhile, after immersion for 14 days, no adhesive trace was observed (**Figure 14(d)**). When the coating layer was damaged by corrosion, relative motion occurred, the coating microstructure was damaged significantly, and cracks were observed on the remaining surface.

As shown in **Figure 14(b)**, weak adhesive traces, wear debris, and fragments were observed on the worn surface of the Al-6Si coating. The worn surface of the corroded coating exhibited in **Figure 14(e)** contained small tear debris, traces of cracks, and delamination. Cracks occurred along the delamination trace owing to fatigue wear. Cracks occurred straightforwardly owing to the pitting corrosion generated during immersion. Moreover, a local shear stress was applied strongly to the corresponding part during the wear test, thereby propagating the cracks and causing delamination. In **Figure 14(c)**, in the case of the uncorroded Al-12Si coating, deep grooves can be observed. This indicates the occurrence of abrasive wear. High-hardness materials exhibit a
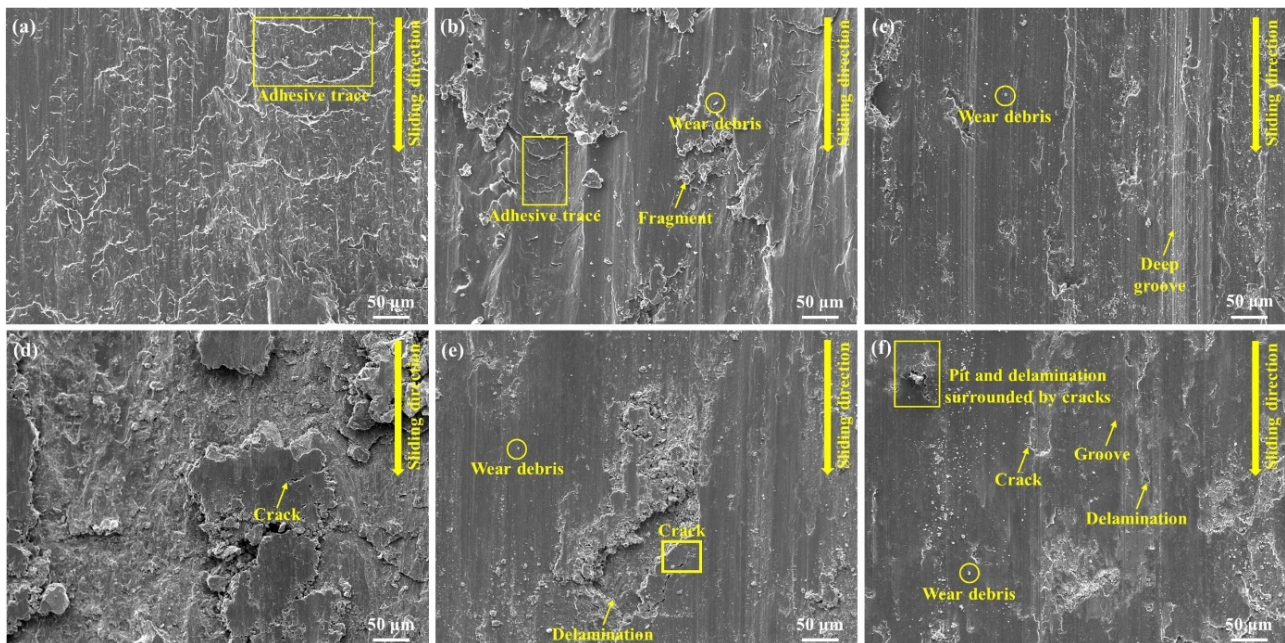

Figure 14: Worn surface of uncorroded coatings: (a)Al, (b)Al-6Si, (c)Al-12Si; and corroded coatings: (d)Al, (e)Al-6Si, (f)Al-12Si

Minhye Kang・Hansol Kwon・Eungsun Byon・Eunkyung Lee

reduced resistance to abrasive wear. The Al-12Si coating had the highest hardness value of 179 HV. Meanwhile, its resistance to abrasive wear was lower than those of the Al and Al-6Si coatings. As shown in **Figure 14(f)**, grooves were also observed on the worn surface of the coating layer immersed for 14 days. In addition, the pits, delamination, and cracks generated by pitting corrosion existed in conjunction. Microcracks and small delamination traces were observed on the edge of the pit. Therefore, it is considered that fatigue wear occurred owing to the rapid propagation of cracks owing to pitting corrosion, similar to the corroded Al-6Si coating.

4. Conclusion

This study investigated the corrosion and wear behaviors of wire arc-sprayed Al and Al-Si coatings on low-carbon steel for application in marine environments.

(1) The coating layers had a microstructure consisting of aluminum oxide and porosity. Microstructural analyses showed that the porosity area fraction of the coatings increased with the Si content. On the Al-Si coating surface, different distributions of eutectic Si were observed in different splats owing to the cooling rate during the coating process.

(2) The cyclic potentiodynamic polarization test indicated that the Al-Si coating was less resistant to pitting corrosion than the Al coating. The Al-12Si coating exhibited a better corrosion resistance than the Al and Al-6Si coatings based on immersion tests. It is attributed to the dense eutectic Si, which obstructs corrosion from permeating through the α-Al matrix.

(3) For the Al-12Si coating, the wear rates were the lowest under both uncorroded and corroded conditions. The corroded Al-Si coatings exhibited fatigue wear. The pits generated during the immersion test weakened the coating surface, thereby causing crack propagation. Consequently, fatigue wear occurred.

Acknowledgements

Author Contributions

Conceptualization, M. Kang and E. Lee; Methodology, M. Kang; Software, M. Kang; Formal Analysis, M. Kang; Investigation, M. Kang, H Kwon, E. Byon and E. Lee; Resources, M. Kang; Data Curation, M. Kang; Writing—Original Draft Preparation, M. Kang; Writing—Review & Editing, E. Byon and E. Lee; Visualization, M. Kang; Supervision, E. Lee; Project Administration, E. Lee; Funding Acquisition, E. Lee.

References

[1] S. Amin and H. Panchal, "A review on thermal spray coating processes," Transfer, vol. 2, no. 4, pp. 556-563, 2016.

[2] M. R. Dorfman, "Thermal spray basics," Advanced Materials & Processes, vol. 160, no. 7, pp. 47-51, 2002.

[3] D. Garcia-Alonso, N. Serres, C. Demian, S. Costil, C. Langlade, and C. Coddet, "Pre-/during-/post-laser processes to enhance the adhesion and mechanical properties of thermal-sprayed coatings with a reduced environmental impact," Journal of Thermal Spray Technology, vol. 20, no. 4, pp. 719-735, 2011.

[4] P. Fauchais and A. Vardelle, "Thermal sprayed coatings used against corrosion and corrosive wear," Advanced plasma spray applications, 2012.

[5] V. R. S. Sá Brito, I. N. Bastos, and H. R. M. Costa, "Corrosion resistance and characterization of metallic coatings deposited by thermal spray on carbon steel," Materials & Design, vol. 41, pp. 282-288, 2012.

[6] C. Senderowski, W. Rejmer, and P. Bilko, "Effect of low chloride and sulfate concentrations on corrosion behavior of aluminum and zinc arc thermal sprayed coatings," Coatings, vol. 12, no. 5, p. 653, 2022.

[7] D. Ferdian, Y. Pratesa, I. Togina, and I. Adelia, "Development of Al-Zn-Cu alloy for low voltage aluminum sacrificial anode," Procedia Engineering, vol. 184, pp. 418-422, 2017.

[8] Y. S. Choi, D. H. Shin, and J. G. Kim, "Sacrificial anode cathodic protection of aluminum-coated steel for automotive mufflers," Corrosion, vol. 63, no. 6, pp. 522-528, 2007.

[9] J. Ryl, J. Wysocka, M. Jarzynka, A. Zielinski, J. Orlikowski, and K. Darowicki, "Effect of native air-formed oxidation on the corrosion behavior of AA 7075 aluminum alloys," Corrosion Science, vol. 87, pp. 150-155, 2014.

[10] H. Allachi, F. Chaouket, and K. Draoui, "Corrosion inhibition of AA6060 aluminium alloy by lanthanide salts in chloride solution," Journal of Alloys and Compounds, vol. 475, no. 1-2, pp. 300-303, 2009.

[11] Z. Szklarska-Smialowska, "Pitting corrosion of aluminum," Corrosion Science, vol. 41, no. 9, pp. 1743-1767, 1999.

[12] M. K. Surappa, S. V. Prasad, and P. K. Rohatgi, "Wear and abrasion of cast Al-alumina particle composites," Wear, vol. 77, no. 3, pp. 295-302, 1982.

[13] W. Jiang, G. Li, Y. Wu, X. Liu, and Z. Fan, "Effect of heat treatment on bonding strength of aluminum/steel bimetal produced by a compound casting," Journal of Materials Processing Technology, vol. 258, pp. 239-250, 2018.

[14] G. Li, W. Jiang, Z. Fan, Z. Jiang, X. Liu, and F. Liu, "Effects of pouring temperature on microstructure, mechanical properties, and fracture behavior of Al/Mg bimetallic composites produced by lost foam casting process," The International Journal of Advanced Manufacturing Technology, vol. 91, no. 1, pp. 1355-1368, 2017.

[15] M. Elmadagli, T. Perry, and A. T. Alpas, "A parametric study of the relationship between microstructure and wear resistance of Al–Si alloys," Wear, vol. 262, no. 1-2, pp. 79-92, 2007.

[16] W. X. Shi, B. Gao, G. F. Tu, and S. W. Li, "Effect of Nd on microstructure and wear resistance of hypereutectic Al–20% Si alloy," Journal of Alloys and Compounds, vol. 508, no. 2, pp. 480-485, 2010.

[17] X. Gu, J. Zhang, X. Fan, N. Dai, Y. Xiao, and L. -C. Zhang, "Abnormal corrosion behavior of selective laser melted AlSi10Mg alloy induced by heat treatment at 300 °C." Journal of Alloys Compounds, vol. 803, pp. 314-324, 2019.

[18] T. Rubben, R. I. Revilla, and I. De Graeve, "Influence of heat treatments on the corrosion mechanism of additive manufactured AlSi10Mg," Corrosion Science, vol. 147, pp. 406-415, 2019.

[19] S. M. A. Shibli, B. N. Meena, and R. Remya. "A review on recent approaches in the field of hot dip zinc galvanizing process," Surface and Coatings Technology, vol. 262, pp. 210-215, 2015.

[20] K. M. Fleming, A. Zhu, and J. R. Scully, "Corrosion of AA6061 brazed with an Al-Si alloy: Effects of Si on metallurgical and corrosion behavior," Corrosion, vol. 68, no. 12, pp. 1126-1145, 2012.

[21] V. Vijeesh and K. Narayan Prabhu, "Review of microstructure evolution in hypereutectic Al–Si alloys and its effect on wear properties," Transactions of the Indian Institute of Metals, vol. 67, no. 1, pp. 1-18, 2014.

[22] A. Vencl, I. Bobić, and Z. Mišković, "Effect of thixocasting and heat treatment on the tribological properties of hypoeutectic Al–Si alloy," Wear, vol. 264, no. 7-8, pp. 616-623, 2008.

[23] A. Mahato, X. Shuman, T. Perry, A. Sachdev, and S. K. Biswas, "Role of silicon in resisting subsurface plastic deformation in tribology of aluminium–silicon alloys," Tribology International, vol. 43, no. 1-2, pp. 381-387, 2010.

[24] M. Warmuzek, Aluminum-Silicon Casting Alloys: An Atlas of Microfractographs: ASM international, 2004.

[25] M. Vardelle, A. Vardelle, A. C. Leger, P. Fauchais, and D. Gobin, "Influence of particle parameters at impact on splat formation and solidification in plasma spraying processes," Journal of Thermal Spray Technology, vol. 4, no. 1, pp. 50-58, 1995.

[26] M. Qian, D. Li, S. B. Liu, and S. L. Gong, "Corrosion performance of laser-remelted Al–Si coating on magnesium alloy AZ91D," Corrosion Science, vol. 52, no. 10, pp. 3554-3560, 2010.

[27] D. J. Varacelle, D. P. Zeek, V. Zanchuck, E. Sampson, K. W. Couch, D. Benson, and G. S. Cox, "Experimental studies of twin-wire electric arc sprayed zinc/aluminum alloy coatings," Journal of Thermal Spray Technology, vol. 7, pp. 513-520, 1998.

[28] D. Thirumalaikumarasamy, K. Shanmugam, and V. Balasubramanian, "Influences of atmospheric plasma spraying parameters on the porosity level of alumina coating on AZ31B magnesium alloy using response surface methodology," Progress in Natural Science: Materials International, vol. 22, no. 5, pp. 468-479, 2012.

[29] S. H. Zahiri, D. Fraser, S. Gulizia, and M. Jahedi, "Effect of processing conditions on porosity formation in cold gas dynamic spraying of copper," Journal of Thermal Spray Technology, vol. 15, no. 3, p. 422, 2006.

[30] M. Kamran, F. Hussain, R. Ahmad, T. Ahmad, F. Riaz, "Investigating the pitting resistance of 316 stainless steel in Ringer's solution using the cyclic polarization technique," Defect and Diffusion Forum, vol. 344, pp. 1-7, 2013.

[31] G. -D. Park, J. H. Yang, K. -H. Lee, H. -J. Kim, S. -H. Lee, J. Kang, Y. -S. Yun, and M. -H. Lee, "Ultra-high corrosion

Minhye Kang · Hansol Kwon · Eungsun Byon · Eunkyung Lee

resistance of Al-Mg-Si film on steel sheet formed by PVD Mg coating and heat treatment," Corrosion Science, vol. 192, 2021.

[32] J. -M. Hu, L. Liu, J. -Q. Zhang, and C. -N. Cao, "Electro-deposition of silane films on aluminum alloys for corrosion protection," Progress in Organic Coatings, vol. 58, no. 4, pp. 265-271, 2007.

[33] M. -C. Zhao, P. Schmutz, S. Brunner, M. Liu, G. Song, and A. Atrens, "An exploratory study of the corrosion of Mg alloys during interrupted salt spray testing," Corrosion Science, vol. 51, no. 6, pp. 1277-1292, 2009.

[34] M. N. Sanath, C. L. Nihal, P. M. Shivaprasad, H. V. Puneeth, and M. K. Srinath, "Review on corrosion studies of heat treated Al-Si alloy," IOP Conference Series: Materials Science and Engineering, vol. 1258, no. 1, 2022.